Indices to Evaluate the Performance of Force Transmission and Constraint for Parallel Mechanisms

Tie Zhang* – Yachao Cao – Guangcai Ma

South China University of Technology, School of Mechanical and Automotive Engineering, China

The force transmission and constraint ability significantly influence the performance of parallel mechanisms (PMs), such as force dexterity, overall rigidity and accuracy. The transmission wrench screw (TWS) transmits the force between the actuator and end-effector, and the constraint wrench screw (CWS) resists structural deformations. They significantly influence the manipulability to transmit force and the consistency to resist deformations. In this study, two new indices are proposed to evaluate their manipulability and consistency. The indices are notable for their unit homogeneity, frame independence, and measurement facility without interference. By taking three PMs with different mobility properties as examples, the effectiveness of the two indices for evaluating the manipulability to transmit force and the consistency to resist deformations is verified. Based on the indices, the configuration of a 3-CRU (C a cylindrical joint, R a revolute joint, and U a universal joint) PM with optimal force transmission and constraint ability is constructed.
Keywords: force transmission manipulability, force constraint consistency, transmission wrench screw, constraint wrench screw, parallel mechanism

Highlights
- *Two new indices with advantages are proposed to evaluate their manipulability and consistency.*
- *The corresponding formulas are derived under different transmission and constraint matrices.*
- *Simulations of three different PMs are carried out to verify the effectiveness of the two indices.*
- *The structural configuration of the 3-CRU PM whose TMI and CCI remain maximal is constructed.*

0 INTRODUCTION

Parallel mechanisms (PMs) have been wide industrial applications due to their merits such as high load-to-weight ratio [1], compact structure [2], good accuracy [3] and dynamic performance [4]. Performance evaluation helps to measure the practical value of PMs before their application. In general, the performance evaluation indices are based on the Jacobian matrix and power to describe the motion and force performance as a whole evaluation index system. The determinant value of the Jacobian matrix as the force transmission index was adopted first by Denavit et al. [5]. Subsequently, performance indices based on the Jacobian matrix were proposed, such as manipulability measure [6], global conditioning index [7], and so on. However, both Merlet [8] and Wang et al. [9] pointed out that these indices are not suitable for the PMs with both rotational and translational degrees of freedom (DoFs). In 1932, the concept of transmission angle was first proposed by Alt [10]. The standardized form of transmission index was put forward by Sutherland and Roth [11], and then it was improved by Tsai and Lee [12]. Furthermore, an input and output transmission index [13] was introduced to describe the motion/force transmission performance of parallel manipulators. A general and systematic method described the motion/force transmissibility of redundantly actuated and over-constrained PMs [14]. Moreover, a modified output transmission index based on an equivalent transmission wrench screw was defined to evaluate the transmissibility of high-speed articulated-platform parallel robots [15].

Highly dynamic handling tasks cannot work properly without good force transmission and constraint performance. Many scholars have extensively studied the force performance of PMs. A new method based on pressure angle describes the force transmission and constraint properties of Delta PM [16]. Wang et al. [17] proposed a new index to assess the relationship between input and output forces. Static actuation force sensitivity was defined to measure the variation of driving forces with the manipulability of external force of the end-effector [18]. Utenov et al. [19] analysed the mapping from the constraint loads in the links to the distributed dynamic loads. Liang and Takeda [20] presented a new transmission index for force constraint evaluation based on the concept of pressure angle. It is widely known that a transmission wrench screw (TWS) transmits the motion and force between actuator and end-effector and a constraint wrench screw (CWS) resists structural deformations. They significantly influence the manipulability to transmit force and the consistency to resist deformations. However, most force transmission indices vary with the coordinate

frame, which may result in biased measure for the same PM due to the selection of different reference coordinate frames. Furthermore, the existing indices only measure the transmissibility of single limb but not a whole PM, and some of them are not homogeneous. However, relatively little literature on force constraint and the consistency to resist deformations could be found.

In this paper, a generalized approach to analysing and evaluating the manipulability to transmit force and the consistency to resist deformations of PM is put forward, in which two indices, namely the force transmission manipulability index (TMI) and the force constraint consistency index (CCI), are proposed. These two indices could be used independently or be used as an auxiliary index together with other performance evaluation indices to measure the force transmission and constraint performance of moving platforms in the process of design, motion planning and control of PMs.

This paper is organized as follows: in Section 1, the force balance is analysed, and two indices, namely TMI and CCI, are proposed. In Section 2, a generalized method to evaluate the manipulability to transmit force and the consistency to resist deformations of PM is proposed. The transmission matrix and the constraint matrix are firstly nondimensionalized, and the calculation formulas of TMI and CCI are presented respectively under three different compositions of transmission matrix and constraint matrix, with the frame invariance of the two indices being also proved. In Section 3, the distributions of TMI and CCI of the PMs with different mobility properties in the chosen spatial workspace are discussed, and the manipulability to transmit force and the consistency to resist deformations are analysed, based on which the configuration of a 3-CRU PM with optimal force transmission and constraint ability is constructed firstly. Section 4 summarizes three merits of the two indices, while Section 5 gives some additional remarks.

1 METHODS MANIPULABILITY TO TRANSMIT FORCE AND CONSISTENCY TO RESIST DEFORMATIONS

When the moving platform moves with constant velocity, the external six-dimension generalized force $\mathbf{W}$ applied to the moving platform should balance with the actuated transmission force $\mathbf{W}_F$ transmitted to the moving platform by actuated joint from each branch and the structural constraint force $\mathbf{W}_C$ of PM in the equilibrium state of forces. For an n-DoF non-

redundant actuated PM with n actuated joints, the force balance equation is

$$\mathbf{W} = \mathbf{W}_F + \mathbf{W}_C. \tag{1}$$

In the process of force transmission, actuated transmission force $\mathbf{W}_F$ is the resultant force of TWS transmitted to the moving platform through all branches, as shown in Fig. 1, and $\mathbf{W}_F$ can be denoted as

$$\mathbf{W}_F = \sum_{i=1}^{n} \$_{ai} = \sum_{i=1}^{n} f_i \left(\mathbf{s}_{f,i}; \mathbf{r}_{f,i} \times \mathbf{s}_{f,i} + h_{f,i} \mathbf{s}_{f,i} \right),$$
$$i = 1, 2, \ldots, n, \tag{2}$$

where f_i is the magnitude of TWS $\$_{ai}$ in terms of force, $\mathbf{S}_{f,i}$ is the unit direction vector of $\$_{ai}$ of the ith limb, $\mathbf{r}_{f,i}$ is the vector of the force acting point in the global coordinate system, and $h_{f,i}$ is the pitch of $\$_{ai}$.

In the process of force constraint, it is known that CWS is generated by mechanical structure. Assuming that there are C_i CWSs of each branch, as presented in Fig. 1, the structural constraint force $\mathbf{W}_C$ can be expressed as

$$\mathbf{W}_C = \sum_{i=1}^{n} \sum_{j=1}^{C_i} \$_{ci,j} = \sum_{i=1}^{n} \sum_{j=1}^{C_i} c_{i,j} \left(\begin{array}{c} \mathbf{s}_{c,i,j}; \\ \mathbf{r}_{c,i,j} \times \mathbf{s}_{c,i,j} + h_{c,i,j} \mathbf{s}_{c,i,j} \end{array} \right),$$
$$i = 1, 2, \cdots, n; \quad j = 1, 2, \cdots, C_i, \tag{3}$$

where $c_{i,j}$ is the magnitude of CWS $\$_{c,i,j}$ in terms of force; $\$_{c,i,j}$ is the unit direction vector of $\$_{c,i,j}$, $\mathbf{r}_{c,i,j}$ is the vector of the force acting point in the global coordinate system, which is introduced as the physical centre of the passive end joint in the ith limb, and $\mathbf{h}_{c,i,j}$ is the pitch of $\$_{c,i,j}$.
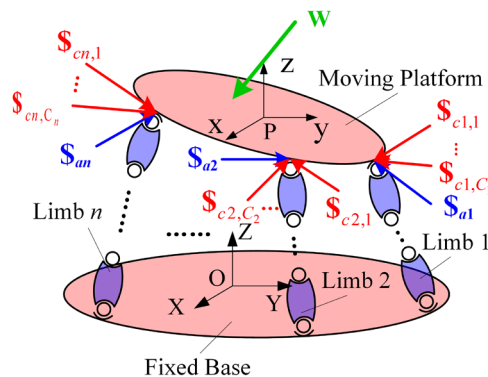
Fig. 1. *Force diagrammatic sketch of PM*

Eqs. (2) and (3) are respectively rewritten as

$$\mathbf{W}_F = \mathbf{Tf}, \tag{4}$$

$$\mathbf{W}_C = \mathbf{Rc}, \tag{5}$$

where $\mathbf{f}=[f_1 \ldots f_n]^T$ denotes the magnitude of the n-dimension force applied by the actuated joint to the moving platform through the branches, $\mathbf{T}$ is the termed transmission matrix [21], and

$$\mathbf{T}=\begin{bmatrix} \mathbf{s}_1 & \mathbf{r}_1 \times \mathbf{s}_1 + h_1\mathbf{s}_1 \\ \vdots & \vdots \\ \mathbf{s}_n & \mathbf{r}_n \times \mathbf{s}_n + h_n\mathbf{s}_n \end{bmatrix}^T_{n\times6}. \qquad (6)$$

$\mathbf{c}=\begin{bmatrix} c_{1,1} & \cdots & c_{1,C_1} & \cdots & c_{n,1} & \cdots & c_{n,C_n} \end{bmatrix}^T$ indicates the magnitude of 6-n dimensional force to resist deformation through the structure of PM when the mechanism is subjected to forces in non-DoF direction. $\mathbf{R}$ is the termed constraint matrix [21] and

$$\mathbf{R}=\begin{bmatrix} \mathbf{s}_{1,1} & \mathbf{r}_{1,1} \times \mathbf{s}_{1,1} + h_{1,1}\mathbf{s}_{1,1} \\ \vdots & \vdots \\ \mathbf{s}_{1,C_1} & \mathbf{r}_{1,C_1} \times \mathbf{s}_{1,C_1} + h_{1,C_1}\mathbf{s}_{1,C_1} \\ \vdots & \vdots \\ \mathbf{s}_{n,1} & \mathbf{r}_{n,1} \times \mathbf{s}_{n,1} + h_{n,1}\mathbf{s}_{n,1} \\ \vdots & \vdots \\ \mathbf{s}_{n,1} & \mathbf{r}_{n,C_n} \times \mathbf{s}_{n,C_n} + h_{n,C_n}\mathbf{s}_{n,C_n} \end{bmatrix}^T_{(6-n)\times6}. \qquad (7)$$

Obviously, the transmission force $\mathbf{W}_F$ depends on the structure of branches and their geometrical arrangement and the constraint force $\mathbf{W}_C$ on the stiffness of the PM (mainly its Young's modulus as well as the lengths and sections of the elements). It should be pointed out that, although the producers of $\mathbf{W}_F$ and $\mathbf{W}_C$ are different, they can still exist simultaneously when the moving platform moves at a uniform velocity, which results in the aggregation of the two matrices in Eq. (1). Each row of these two matrices is just a force or a moment. The force and moment are simply combined into a sum screw according to spinor algebra.

1.1 Force Transmission Manipulability Index

From Eq. (6), it can be seen that transmission matrix $\mathbf{T}$ is composed of TWS, which transmits the forces between actuators in joint space and the end-effectors in operational space. In order to evaluate the sensitivity of mutual disturbance in the process of force transmission, $\mathbf{T}$ is decomposed by means of singular value decomposition (SVD). Assuming $\mathbf{T}$ is homogeneous,

$$\mathbf{T}=\mathbf{U}\mathbf{\Sigma}\mathbf{V}^T, \qquad (8)$$

where $\mathbf{U}$ and $\mathbf{V}$ are respectively $n\times n$ and 6×6 orthogonal matrices, $\mathbf{\Sigma}=[\mathbf{\Sigma}_1 \mathbf{O}]_{n\times6}$, and $\mathbf{\Sigma}_1=\text{diag}(\sigma_1,\sigma_2,...,\sigma_n)$, whose diagonal elements are arranged in the order of $\sigma_1\geq\sigma_2\geq...\geq\sigma_n>0$. $\sigma_1,\sigma_2,...,\sigma_n$ denote the singular values of $\mathbf{T}$. $\mathbf{O}$ denotes zero matrix.

Post-multiply both sides of Eq. (8) by matrix $\mathbf{V}^{-T}\mathbf{\Sigma}^+$, then

$$\mathbf{T}\mathbf{V}^{-T}\mathbf{\Sigma}^+ = \mathbf{U}, \qquad (9)$$

where $\mathbf{\Sigma}^+$ is the pseudo inverse matrix of the diagonal matrix $\mathbf{\Sigma}$, and $\mathbf{\Sigma}^+=\begin{bmatrix} \mathbf{\Sigma}_1^{-1} \\ \mathbf{O} \end{bmatrix}_{6\times n}$ with

$\mathbf{\Sigma}_1^{-1}=\text{diag}(1/\sigma_1,1/\sigma_2,\cdots,1/\sigma_n)$.

Rewrite matrix $\mathbf{V}^{-T}\mathbf{\Sigma}^+$ as

$$\mathbf{V}^{-T}\mathbf{\Sigma}^+=\begin{pmatrix} \tilde{\mathbf{v}}_1/\sigma_1 & \cdots & \tilde{\mathbf{v}}_n/\sigma_n \end{pmatrix}, \qquad (10)$$

where $\tilde{\mathbf{v}}_n$ represents the nth column of matrix $\mathbf{V}^{-T}$.

From the physical meaning of SVD, it can be seen that $f_n=\|\tilde{\mathbf{v}}_n/\sigma_n\|$. Combined with Eq. (4), the following equation exists:

$$\mathbf{W}_F = \mathbf{T}\mathbf{f} = \mathbf{T}\begin{pmatrix} f_1 \\ \vdots \\ f_n \end{pmatrix}=\mathbf{T}\begin{pmatrix} \|\tilde{\mathbf{v}}_1/\sigma_1\| \\ \vdots \\ \|\tilde{\mathbf{v}}_n/\sigma_n\| \end{pmatrix}. \qquad (11)$$

Then, the "elastic" ratio Γ can be defined as the 2-norm ratio of $\mathbf{f}$ to $\mathbf{W}_F$, that is,

$$\Gamma=\frac{\|\mathbf{W}_F\|}{\|\mathbf{f}\|}=\frac{1}{\sqrt{\sum_{i=1}^{n}1/\sigma_i^2}}. \qquad (12)$$

The physical meaning of Γ is the "elastic" length after $\mathbf{f}$ in joint space is rotation-, scaling- and projection-transformed into $\mathbf{W}_F$ in operational space, which reflects the manipulability of actuated force. Thus, it can be called as force transmission manipulability ratio. Γ ranges from 0 to Γ_{max}. When all σ_i are equal each other, Γ equals to the maximum, and the force transmission manipulability behaves the best; When Γ is close to 0, the force transmission manipulability behaves the worst and then force transmission singularity may occur.

To normalize the ratio, by comparing and measuring Γ in different poses intuitively, force transmission manipulability index (TMI) is defined as

$$\rho_\Gamma=\Gamma/\Gamma_{\text{max}}. \qquad (13)$$

The closer ρ_Γ gets to 1, the less distortion $\mathbf{f}$ has, which means that the TWSs exerted on the moving platform have no distortion and that the manipulability

of transmission force is excellent. When ρ_Γ approaches zero, $\mathbf{f}$ extends or shrinks to infinity after the transformation, and actuation singularity is encountered.

1.2 Force Constraint Consistency Index

Constraint matrix $\mathbf{R}$ is composed of CWS, which counterbalances the external forces and resists deformations. The SVD and relevant derivation process of the homogeneous constraint matrix $\mathbf{R}$ is similar to $\mathbf{T}$, and the force constraint consistency ratio can be expressed as

$$\Omega = \frac{\|\mathbf{W}_C\|}{\|\mathbf{c}\|} = \frac{1}{\sqrt{\sum_{i=1}^{6-n} 1/\sigma_i^2}}. \tag{14}$$

Force constraint consistency index (CCI) is expressed as

$$\rho_\Omega = \Omega/\Omega_{\max}. \tag{15}$$

The closer ρ_Ω is to 1, the more stable $\mathbf{c}$ is, which means that the CWSs exerted on the moving platform have less "elastic" change and basically keep consistent, and that the consistency of force constraint is excellent. When ρ_Ω is near to zero, $\mathbf{c}$ extends or shrinks to infinity after the transformation, and constraint singularity is encountered.

2 SOLUTION OF FORCE TRANSMISSION MANIPULABILITY RATIO AND CONSTRAINT CONSISTENCY RATIO

To calculate $\Gamma_{\max}$ and $\Omega_{\max}$, $\mathbf{T}$ and $\mathbf{R}$ need to be solved first. In this section, the corresponding calculation models of $\Gamma_{\max}$ and $\Omega_{\max}$ are discussed based on the possible composition of the transmission matrix $\mathbf{T}$ and constraint matrix $\mathbf{R}$ presented in Table 1. Then, ρ_Γ and ρ_Ω in six cases are respectively derived.

Table 1. *The possible composition of the transmission matrix and constraint matrix*

	Transmission matrix $\mathbf{T}$	Constraint matrix $\mathbf{R}$
Only composed of linear force vectors	Section 2.2.1	Section 2.3.1
Only composed of force couples	Section 2.2.2	Section 2.3.2
Composed of both linear force vectors and force couples	Section 2.2.3	Section 2.3.3

2.1 Homogenization of Transmission Matrix and Constraint Matrix

When $\mathbf{T}$ and $\mathbf{R}$ are composed of only linear force vectors or both linear force vectors and force couples, the dimensions of the left three columns and the right three columns elements of $\mathbf{T}$ and $\mathbf{R}$ are different. Therefore, these two matrices should be homogenized before SVD.

2.1.1 Homogeneous Transmission Matrix

The three right column elements of $\mathbf{T}$ are multiplied by a characteristic length L_ξ [22] to unify the dimension. In this case, the homogeneous transmission matrix $\mathbf{T}_h$ is

$$\mathbf{T}_h = \begin{bmatrix} \mathbf{T}_1 & \mathbf{T}_2/L_\xi \end{bmatrix}, \tag{16}$$

where $\mathbf{T}_1 = [\mathbf{s}_1 \dots \mathbf{s}_n]^T$, and $\mathbf{T}_2 = [(\mathbf{r}_1 \times \mathbf{s}_1) \dots (\mathbf{r}_n \times \mathbf{s}_n)]^T$, the isotropy condition for $\mathbf{T}_h$ is

$$\mathbf{T}_h{}^T \mathbf{T}_h = \begin{bmatrix} \mathbf{T}_1{}^T \mathbf{T}_1 & (\mathbf{T}_1{}^T \mathbf{T}_2)/L_\xi \\ (\mathbf{T}_2{}^T \mathbf{T}_1)/L_\xi & (\mathbf{T}_2{}^T \mathbf{T}_2)/L_\xi{}^2 \end{bmatrix} = \sigma_\xi{}^2 \mathbf{I}, \tag{17}$$

where $\sigma_\xi > 0$ is a nondimensional scalar and $\mathbf{I}$ is a 6×6 identity matrix. When $\mathbf{T}_h$ is isotropic, the singular values of $\mathbf{T}_h$ are identical. At this time, the PM has at least one configuration in the whole workspace [21]. Furthermore, if $\mathbf{T}_h$ does not satisfy the isotropy condition, i.e., the PM cannot reach an isotropy configuration, it is necessary to seek a configuration over the whole workspace in which the condition number reaches the minimum.

Based on the Frobenius norm, the condition number of $\mathbf{T}_h$ is calculated as [23]

$$\kappa(\mathbf{T}_h) = \|\mathbf{T}_h\|_F \|\mathbf{T}_h{}^{-1}\|_F = \frac{1}{6}\sqrt{\mathrm{tr}(\mathbf{T}_h{}^T \mathbf{T}_h)\mathrm{tr}[(\mathbf{T}_h{}^T \mathbf{T}_h)^{-1}]}. \tag{18}$$

To solve L_ξ, $\kappa^2(\mathbf{T}_h)$ is minimized. Thus, the objective function subjected to the corresponding geometric constraints is

$$\min_{\mathbf{x}} \kappa^2(\mathbf{T}_h). \tag{19}$$

The design vector $\mathbf{x}$ is related to configuration variables $\boldsymbol{\Phi}$ of end-effector and L_ξ, namely $\mathbf{x} = [\boldsymbol{\Phi} \; L_\xi]$. Therefore, the above solution can be represented as

$$\begin{aligned} &\underset{\mathbf{x}}{\text{minimize}} && \kappa^2(\mathbf{T}_h) \\ &\text{subject to} && \boldsymbol{\Phi} \in \mathbf{S} \end{aligned}, \tag{20}$$

where $\mathbf{S}$ denotes the workspace of the PM.

By computing the optimization problem, the characteristic length L_ξ can be obtained, thus obtaining

the homogeneous transmission matrix $\mathbf{T}_h$. For the sake of simplicity, the dimensionless coefficient of transmission matrix and constraint matrix here are derived only by taking the linear force vector as an example. When the matrix is composed of both linear force vectors and force couples, the deduction process is similar.

2.1.2 Homogeneous Constraint Matrix

Similarly, to unify the dimension of $\mathbf{R}$, a characteristic length L_η is calculated by

$$\begin{array}{ll} \underset{\mathbf{x}}{\text{minimize}} & \kappa^2(\mathbf{R}_h) \\ \text{subject to} & \mathbf{\Phi} \in \mathbf{S} \end{array}, \qquad (21)$$

where $\kappa(\mathbf{R}_h) = \dfrac{1}{6}\sqrt{\text{tr}(\mathbf{R}_h{}^T\mathbf{R}_h)\,\text{tr}[(\mathbf{R}_h{}^T\mathbf{R}_h)^{-1}]}$ and $\mathbf{R}_h$ is represented by L_η.

2.2 Calculation Formula of TMI

2.2.1 Transmission Matrix Composed of linear Force Vectors

When $\mathbf{T}$ is only composed of linear force vectors, the dimensionless transmission matrix $\mathbf{T}_h$ is

$$\mathbf{T}_h = \begin{bmatrix} \mathbf{s}_1 & (\mathbf{r}_1 \times \mathbf{s}_1)\ /L_\xi \\ \vdots & \vdots \\ \mathbf{s}_n & (\mathbf{r}_n \times \mathbf{s}_n)\ /L_\xi \end{bmatrix}^T. \qquad (22)$$

The trace of matrix $\mathbf{T}_h{}^T\mathbf{T}_h$ is solved as $\text{tr}(\mathbf{T}_h{}^T\mathbf{T}_h) = \sum_{i=1}^n \sigma_i^2 = n + \sum_{i=1}^n \dfrac{1}{L_\xi^2}(\mathbf{r}_i \times \mathbf{s}_i)^2$. When $\sigma_i^2 = k/n$, the transmission manipulability ratio Γ achieves the maximum $\sqrt{k/n}$. Therefore, TMI can be calculated by

$$\rho_\Gamma = \frac{n}{\sqrt{(n + \sum_{i=1}^n \frac{1}{L_\xi^2}\|\mathbf{r}_i \times \mathbf{s}_i\|^2)\sum_{i=1}^n \frac{1}{\sigma_i^2}}}. \qquad (23)$$

2.2.2 Transmission Matrix Composed of Force Couples

When $\mathbf{T}$ is only composed of force couples, TMI can be calculated as

$$\rho_\Gamma = \sqrt{\frac{n}{\sum_{i=1}^n \frac{1}{\sigma_i^2}}}. \qquad (24)$$

2.2.3 Transmission Matrix Composed of Linear Force Vectors and Force Couples

When $\mathbf{T}$ is composed of m linear force vectors and n-m force couples, TMI is

$$\rho_\Gamma = \frac{n}{\sqrt{(n + \sum_{i=1}^m (\frac{1}{L_\xi^2}\|\mathbf{r}_i \times \mathbf{s}_i\|^2))\sum_{i=1}^n \frac{1}{\sigma_i^2}}}. \qquad (25)$$

2.3 Calculation Formula of CCI

2.3.1 Constraint Matrix Composed of Linear Force Vectors

When $\mathbf{R}$ is only composed of linear force vectors, CCI can be calculated as

$$\rho_\Omega = \frac{6-n}{\sqrt{\left(\sum_{i=1}^{6-n} C_i + \sum_{i=1}^{6-n}\sum_{j=1}^{C_i} \frac{1}{L_\eta^2}(\mathbf{r}_{i,j} \times \mathbf{s}_{i,j})^2\right)\sum_{i=1}^{6-n} 1/\sigma_i'^2}}. \qquad (26)$$

It should be noted that there are $\sum_{i=1}^n \sum_{j=1}^{6-C_i} j$ ($j = 1, 2, ..., 6-C_i$, $i = 1, 2, ..., n$) CWSs. The 6-n DoFs of the moving platform are constrained by these CWSs, that is rank$(\mathbf{R}_h) = 6-n$. It is only necessary to pick up 6-n linearly independent screws from these $\sum_{i=1}^n \sum_{j=1}^{6-C_i} j$ CWSs to compose the constraint matrix.

2.3.2 Constraint Matrix Composed of Force Couples

When $\mathbf{R}$ is only composed of force couples, CCI can be obtained as

$$\rho_\Omega = \frac{6-n}{\sqrt{\sum_{i=1}^{6-n} C_i \sum_{i=1}^{6-n} 1/\sigma_i'^2}}. \qquad (27)$$

2.3.3 Constraint Matrix Composed of Linear Force Vectors and Force Couples

When $\mathbf{R}$ is composed of $\sum_{i=1}^n m_i$ linear force vectors and $\sum_{i=1}^n (C_i - 2m_i)$ force couples, CCI can be calculated as

$$\rho_\Omega = \frac{6-n}{\sqrt{(\sum_{i=1}^{6-n} C_i + \sum_{i=1}^{6-n}(\frac{1}{L_\eta^2}\|\mathbf{r}_{i,j} \times \mathbf{s}_{i,j}\|^2))\sum_{i=1}^{6-n} 1/\sigma_i'^2}}. \qquad (28)$$

2.4 Frame Invariance of TMI and CCI

Assuming that the transmission force is expressed by $\mathbf{W}_F$ in a coordinate system $\{O\}$, in another coordinate system $\{O'\}$, the same transmission force is represented by $\mathbf{W}_F'$. The relationship between the forces in different coordinate frame can be expressed as

$$\left(\mathbf{W}_F^T\right)' = \mathbf{Ad_g}\mathbf{W}_F^T, \tag{29}$$

where $\mathbf{Ad_g}$ is transformation matrix.

Then $\mathbf{W}'$ can be calculated by

$$\left(\mathbf{T}'\right)^T = \mathbf{Ad_g}\mathbf{T}^T\mathbf{Ad_g}^{-1}. \tag{30}$$

By rewriting Eq. (8) into the form of column vector, namely

$$\sigma_i\mathbf{v}_i^T = \mathbf{T}^T\mathbf{u}_i^T \quad i = 1,2,\cdots,n, \tag{31}$$

and pre-multiplying both sides of Eq. (31) by the matrix $\mathbf{Ad_g}$, it can be obtained as

$$\sigma_i\left(\mathbf{v}_i^T\right)' = \mathbf{Ad_g}\mathbf{T}^T\mathbf{Ad_g}^{-1}\left(\mathbf{u}_i^T\right)', \tag{32}$$

where $\left(\mathbf{v}_i^T\right)' = \mathbf{Ad_g}\mathbf{v}_i^T$ and $\left(\mathbf{u}_i^T\right)' = \mathbf{Ad_g}\mathbf{u}_i^T$. In other words, vectors $\mathbf{v}_i^T$ and $\mathbf{u}_i^T$ in the frame $\{O\}$ are transformed into $\left(\mathbf{v}_i^T\right)'$ and $\left(\mathbf{u}_i^T\right)'$ in the frame $\{O'\}$, respectively.

Substituting Eq. (30) into Eq. (32) yields

$$\sigma_i\left(\mathbf{v}_i^T\right)' = \left(\mathbf{T}^T\right)'\left(\mathbf{u}_i^T\right)'. \tag{33}$$

Comparing Eq. (31) with Eq. (33), it can be seen that the singular values of $\mathbf{T}'$ and $\mathbf{T}$ are identical in different coordinate frames. The coordinate transformation of the transmission matrix does not affect its singular value. In the same way, it can be proved that constraint matrix $\mathbf{R}$ also has this property. From Eqs. (12) to (15), it can be seen that neither TMI nor CCI varies with the reference coordinate frame. This property is called the frame invariance of TMI and CCI.

3 MANIPULABILITY OF TRANSMISSION FORCE AND CONSISTENCY OF CONSTRAINT FORCE ANALYSIS OF PMS WITH DIFFERENT MOBILITY PROPERTIES

In this section, TMI and CCI for several typical PMs will be calculated to illustrate the usage of the two indices as well as the manipulability to transmit force and the consistency to resist deformations of the PMs.

3.1 4-URU Three-Translational and One-Rotational PM with Mixed-Motion

The sketch of 4-URU PM [24] are shown in Fig. 2. The mobility properties are three translational DoFs and one rotational DoF around the z-axis. The rotation angle of the moving platform around z-axis is represented by α. The horizontal revolute joint of the universal joint A_i is actuated.

The moving platform of the 4-URU PM is exerted by four constraint couples from four branches, and the constraint matrix is

$$\mathbf{R}_0 = \begin{bmatrix} \mathbf{s}_{r1}^T & \mathbf{s}_{r2}^T & \mathbf{s}_{r3}^T & \mathbf{s}_{r4}^T \end{bmatrix}, \tag{34}$$

where $\mathbf{s}_{ri}(i=1,2,3,4)$ denotes the direction vectors of the constraint couples, which are in parallel with the plane of the moving platform.
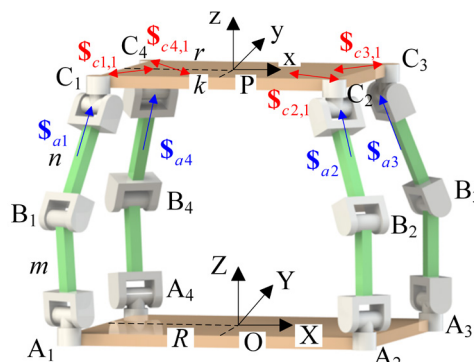
Fig. 2. Sketch of 4-URU PM

Since the four constraint couples are all in one plane, $\mathbf{R}_0(:,3)=\mathbf{0}$. In addition, only two force couples are linearly independent based on the dependence of screw system [25]. That is to say, $\mathbf{s}_{r3}^T$ and $\mathbf{s}_{r4}^T$ can be linearly represented by $\mathbf{s}_{r1}^T$ and $\mathbf{s}_{r2}^T$. Therefore, the constraint matrix is rewritten as

$$\mathbf{R}_h = \begin{bmatrix} \mathbf{R}_0(1,1:2) \\ \mathbf{R}_0(2,1:2) \end{bmatrix}. \tag{35}$$

Obviously, $\mathbf{R}_h$ is homogeneous matrix.

When the actuated joints are locked, the transmission matrix is

$$\mathbf{T}_0 = \begin{bmatrix} \mathbf{r}_{a1} \times \mathbf{s}_{a1} & \mathbf{s}_{a1} \\ \mathbf{r}_{a2} \times \mathbf{s}_{a2} & \mathbf{s}_{a2} \\ \mathbf{r}_{a3} \times \mathbf{s}_{a3} & \mathbf{s}_{a3} \\ \mathbf{r}_{a4} \times \mathbf{s}_{a4} & \mathbf{s}_{a4} \end{bmatrix}^T, \tag{36}$$

where $\mathbf{r}_{ai}$ represents the vector of acting point of TWS $\$_i^a$ in fixed coordinate frame $\{O\}$. $\mathbf{S}_{ai}$ denotes the direction vectors of the transmission forces.

From the mobility of the PM, the homogeneous transmission matrix can be written as

$$\mathbf{T}_h = \left[\mathbf{T}_P / L_\xi \quad \mathbf{T}_O\right], \qquad (37)$$

where $\mathbf{T}_P = \begin{bmatrix} \mathbf{T}_0(1,3) \\ \mathbf{T}_0(2,3) \\ \mathbf{T}_0(3,3) \\ \mathbf{T}_0(4,3) \end{bmatrix}$ and $\mathbf{T}_O = \begin{bmatrix} \mathbf{T}_0(1,4:6) \\ \mathbf{T}_0(2,4:6) \\ \mathbf{T}_0(3,4:6) \\ \mathbf{T}_0(4,4:6) \end{bmatrix}$.

The condition number of $\mathbf{T}_h$ is calculated based on Eq. (18), i.e.,

$$\kappa(\mathbf{T}_h) = \left\|\mathbf{T}_h\right\|_F \left\|\mathbf{T}_h^{-1}\right\|_F = \frac{1}{4}\sqrt{\mathrm{tr}(\mathbf{T}_h^T\mathbf{T}_h)\mathrm{tr}[(\mathbf{T}_h^T\mathbf{T}_h)^{-1}]}. \quad (38)$$

To obtain the minimum values of $\kappa(\mathbf{T}_h)$ and L_ξ of the isotropic configuration, the problem becomes

$$\begin{aligned} \underset{\mathbf{x}}{\text{minimize}} \quad & \kappa^2(\mathbf{T}_h) \\ \text{subject to} \quad & \boldsymbol{\Phi} \in \mathbf{S} \end{aligned}. \qquad (39)$$

To determine the optimum solution of problem (39), the structure parameters of the 4-URU PM are given as $R=500$ mm, $r_1=400$ mm, $r_2=300$ mm, $m=700$ mm and $n=800$ mm, the initial design vector $\mathbf{x}$ including both $\boldsymbol{\Phi}$ and L_ξ is assigned as $\mathbf{x}_{init}=[100\,100\,1200\,300]^T$ and the "interior-point" algorithm is adopted, thus obtaining $\mathbf{x}_{opt}=[-25.37\,207.72\,893.57\,723.14]^T$. The fourth element denotes the characteristic length, i.e., $L_\xi=723.14$ mm. By using this value to homogenize the transmission matrix, the minimum condition number is calculated as $\kappa_{min}=1.00$, which means that the characteristic length is available.

By respectively substituting Eqs. (37) and (35) into Eqs. (27) and (23), the equations of TMI and CCI can be deduced as

$$\rho_\Gamma = \frac{4}{\sqrt{(4 + \sum_{i=1}^{4}\frac{1}{L_\xi^2}\mathbf{T}_0(i,3)^2)\sum_{i=1}^{n}\frac{1}{\sigma_i^2}}}, \qquad (40)$$

$$\rho_\Omega = \sqrt{\frac{2}{\sum_{i=1}^{2}1/\sigma_i'^2}}, \qquad (41)$$

where σ_i and σ' are singular values of matrix $\mathbf{T}_h$ and $\mathbf{R}_h$, respectively.

Based on Eqs. (40) and (41), the distributions of TMI and CCI in the chosen spatial workspace are obtained when the rotation angle of the moving platform around z-axis is 0°, as shown in Fig. 3. The values of TMI and CCI are presented in Table 2. The maximum and minimum of TMI are computed as 0.43

and 0, and the maximum and minimum of CCI are 1 and 0.02, respectively.

a)

b)

c)

d)
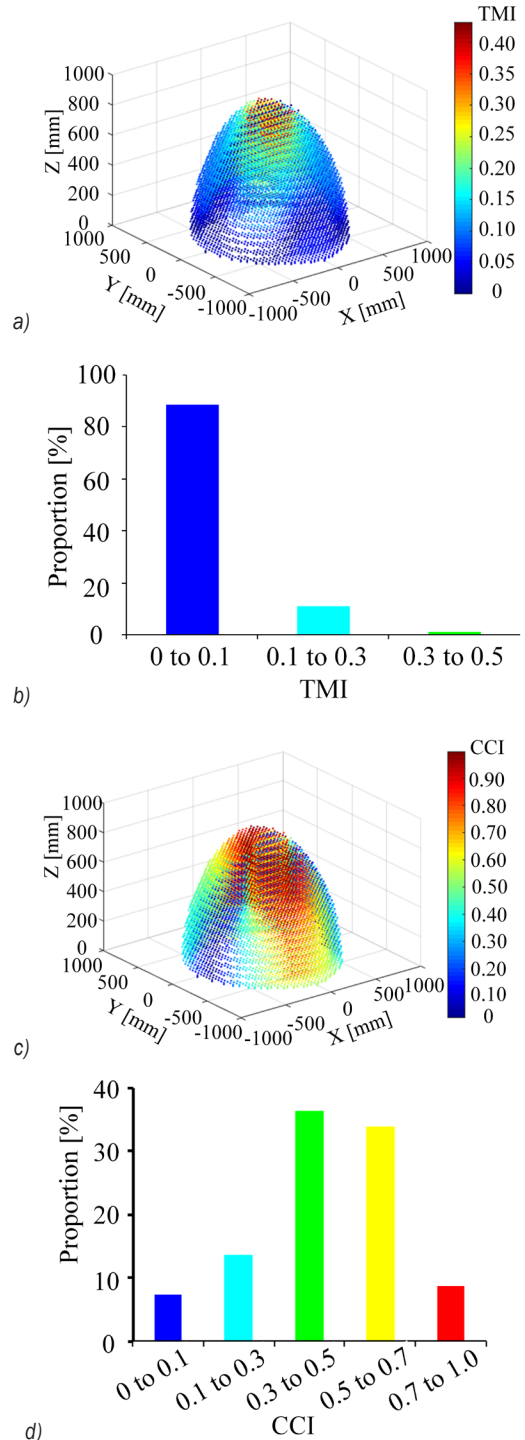
Fig. 3. a) Distribution of the TMI of 4-URU PM when $\alpha=0°$, b) proportion of TMI values in each interval, c) distribution of the CCI of 4-URU PM when $\alpha=0°$, and d) proportion of CCI values in each interval

a)

b)

c)

d)
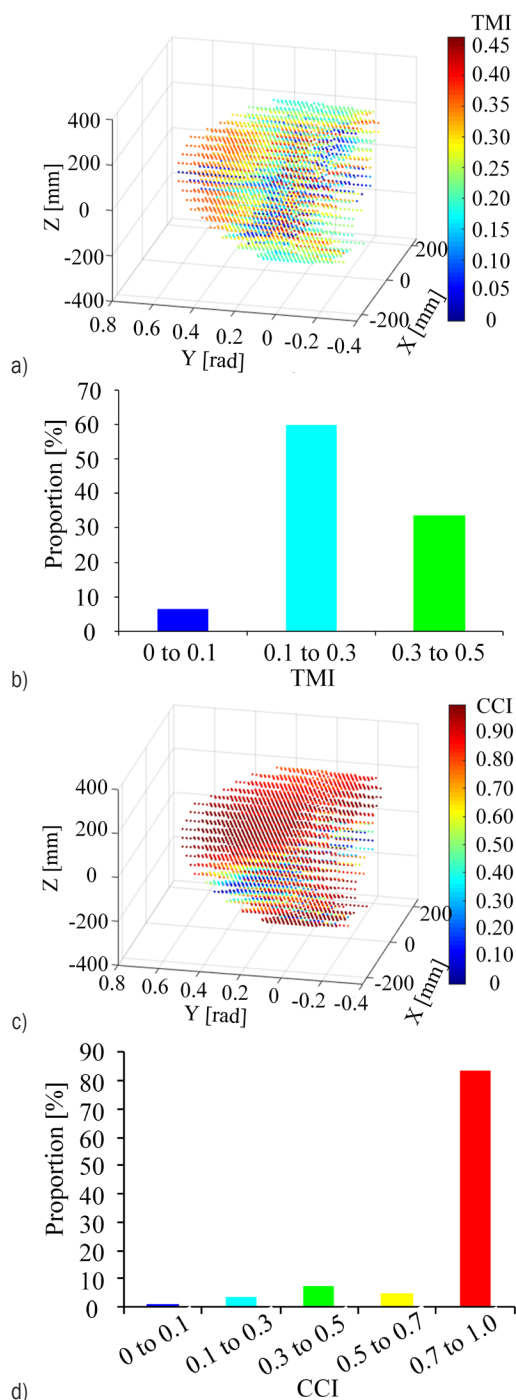
Fig. 4. *a) Distribution of the TMI of 4-URU PM when z_p=900 mm, b) proportion of TMI values in each interval, c) distribution of the CCI of 4-URU PM when z_p=900 mm, and d) proportion of CCI values in each interval*

Fig. 3a illustrates that the closer the centre point P of the moving platform to z-axis, the larger the TMI and the less "elastic" variation of the TWSs applied to the moving platform. On the whole, the majority of

TMI in the chosen spatial workspace is less than 0.1 (see Fig. 3b), meaning that the manipulability of the TWSs is sharply changed and is nearly close to the singularity when $\alpha=0°$. However, CCI is more than 0.5 in most areas of the chosen spatial workspace (see Figs. 3c and d), meaning that the CWSs exerted on the moving platform have less "elastic" variation when the moving platform moves in translational direction. The consistency of the CWS to resist the deformations is moderate.

Table 2. *The values of the proposed parameters of 4-URU PM when $\alpha=0°$*

		TMI	CCI
Maximum		0.43	1
Minimum		0	0.02
Proportion of each interval	0 to 0.1	88.34 %	7.30 %
	0.1 to 0.3	10.79 %	13.71 %
	0.3 to 0.5	0.87 %	36.42 %
	0.5 to 0.7	0	33.89 %
	0.7 to 1.0	0	8.68 %

Table 3. *The values of the proposed parameters of 4-URU PM when z_p=900 mm*

		TMI	CCI
Maximum		0.46	1
Minimum		0	0
Proportion of each interval	0 to 0.1	6.40 %	1.32 %
	0.1 to 0.3	59.95 %	3.24 %
	0.3 to 0.5	33.64 %	7.07 %
	0.5 to 0.7	0	4.70 %
	0.7 to 1.0	0	83.68 %

Fig. 4 shows the distributions of TMI and CCI in the chosen spatial workspace when the translational DoF of the moving platform along z-axis is fixed (z_p = 900 mm). The corresponding values of TMI and CCI are presented in Table 3. The maximum of TMI is 0.46 and the minimum is 0. The maximum of CCI is 1 and the minimum is 0. As shown in Fig. 4a, the larger the angle along y-axis, the larger the TMI and the less "elastic" variation of the TWSs exerted on the moving platform. Moreover, as shown in Fig. 4b, most TMI values in the chosen spatial workspace vary from 0.1 to 0.5. Consequently, by comparing Fig. 3 with Fig. 4, it can be seen that the manipulability variation of the TWSs with 0° of the rotation angle of the moving platform around z-axis is less than that with fixed translational DoF of the moving platform along z-axis. In addition, CCI is more than 0.7 in most areas of the chosen spatial workspace (see Figs. 4c and d), which means that, when the moving platform moving

along z-axis is fixed, the CWSs exerted on the moving platform is of less distortion and the consistency of force constraint behaves well.

3.2 2-UPR+SPR Two-Rotational and One-Translational PM with Parasitic Motion

The 2-UPR+SPR (P a prismatic joint; S a spherical joint.) PM possesses two rotational DoFs round x-axis and y-axis and one translational DoF along z-axis, which is well known as the positioning module of the Exechon parallel machine tool [26]. The rotation angle of the moving platform around x-axis and y-axis are represented by α and β, respectively. The sketch is established as presented in Fig. 5. The prismatic joint B_i is actuated.

The equations of TMI and CCI is

$$\rho_\Gamma = \frac{3}{\sqrt{\left(3 + \sum_{i=1}^{3}\sum_{j=1}^{2}\frac{1}{L_\xi^2}\mathbf{T}_0(i,j)^2\right)\sum_{i=1}^{3}\frac{1}{\sigma_i^2}}}, \quad (42)$$

$$\rho_\Omega = \frac{3}{\sqrt{\left(3 + \sum_{i=1}^{3}\frac{1}{L_\eta^2}\mathbf{R}_0(i,3)^2\right)\sum_{i=1}^{3}\frac{1}{\sigma_i'^2}}}, \quad (43)$$

where the characteristic length $L_\xi = 353.55$ and $L_\eta = 483.80$ according to the computing analysis.
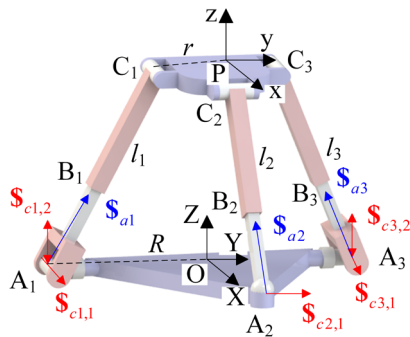
Fig. 5. *Sketch of 2-UPR+SPR PM*

Fig. 6 shows the distributions of TMI and CCI of 2-UPR+SPR PM in the chosen spatial workspace. The corresponding values of TMI and CCI are presented in Table 4. The computed TMI ranges from 0.36 to 1.00, and the computed CCI ranges from 0.26 to 0.62. As shown in Figs. 6a and b, TMI is more than 0.7 in most areas of the workspace, and the TWSs exerted on the moving platform are of less distortion, which means that the manipulability of transmission force is moderate.
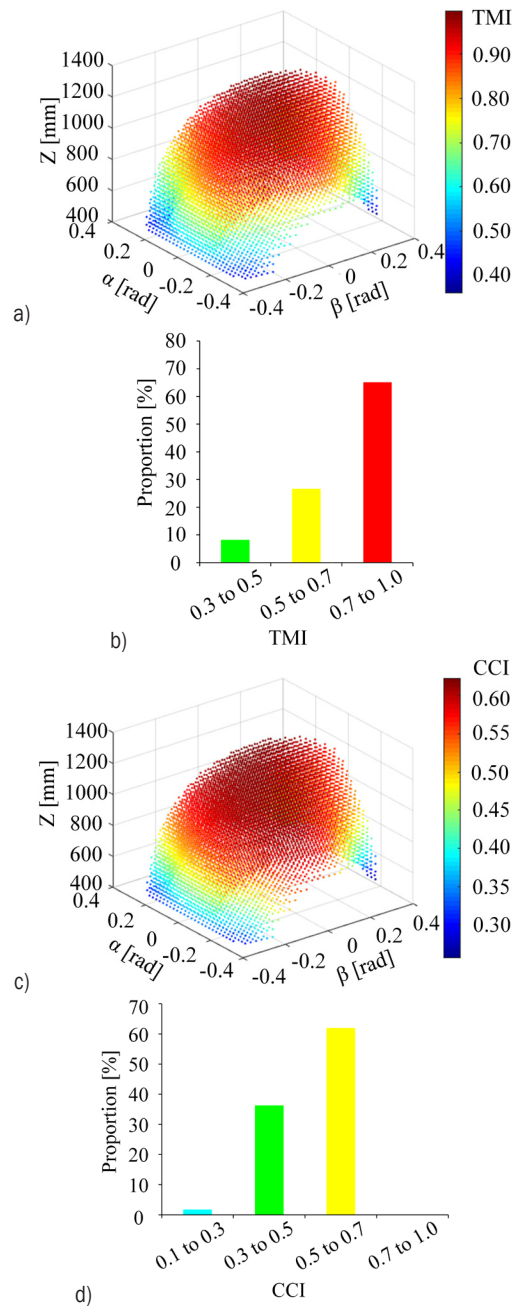
Fig. 6. *a) Distribution of the TMI of 2-UPR+SPR PM, b) proportion of TMI values in each interval, c) distribution of the CCI of 2-UPR+SPR PM, and d) proportion of CCI values in each interval*

Similar with TMI, the majority of CCI is up to 0.50 (see Figs. 6c and d), and the CWSs exerted on the moving platform are also of less "elastic" variation, meaning that the consistency of force constraint is moderate. Furthermore, due to the parasitic motion of the mechanism [27], that is, during its rotation around x-axis and y-axis, the moving platform translates along x-axis and y-axis at the same time. Thus, the

translation DoFs along x-axis and y-axis are not constrained, which brings great difficulty to the control algorithm of the PM. In addition, the existence of the parasitic motion also makes the kinematics calibration of PM very difficult. Parasitic motion is an inherent characteristic of PM and cannot be compensated by its own control system, so that it is often minimized via structural optimization design.

3.3 3-CRU Three-Translational PM with Pure Motion

Fig. 7 shows the sketch of a 3-CRU PM [28] with three translational DoFs. The translation of the cylindrical joint A_i is actuated.
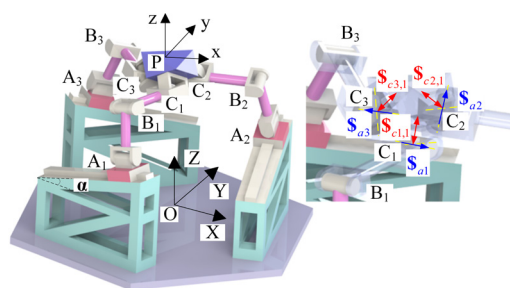
Fig. 7. *Sketch of 3-CRU PM*

Then, TMI and CCI can respectively be calculated by

$$\rho_\Gamma = \sqrt{\frac{3}{\sum_{i=1}^{3} 1/\sigma_i^2}}, \tag{44}$$

$$\rho_\Omega = \sqrt{\frac{3}{\sum_{i=1}^{3} 1/\sigma_i'^2}}. \tag{45}$$

Table 4. *The values of the proposed parameters of 2-UPR+SPR PM*

		TMI	CCI
Maximum		0.36	0.26
Minimum		1.00	0.62
Proportion of each interval	0 to 0.1	0	0
	0.1 to 0.3	0	1.75 %
	0.3 to 0.5	8.21 %	36.28 %
	0.5 to 0.7	26.67 %	61.97 %
	0.7 to 1.0	65.12 %	0

The direction of TWS is parallel with the slide rail and remains constant [28], that is, the transmission matrix remains constant. In addition, the direction of constraint force couple is perpendicular to both axes of the universal joint C_i. The kinematic and constraint

properties of the PM determine that the revolute joint connected with the platform is an inactive joint (The inactive joint reduces the over-constraint of the PM). Thus, the constraint force couple also remains constant, namely, the constraint matrix remains constant. From above-mentioned analysis, it can be found that the transmission linear force vector is only related to the angle α between the slide rail and the base plane. In addition to α, the transmission force couple also depends on the angle β between the edge of the platform and the axis of the R joint B_i. Fig. 8 illustrates these two angles.

Fig. 8. α and β of the ith branch

a)

b)
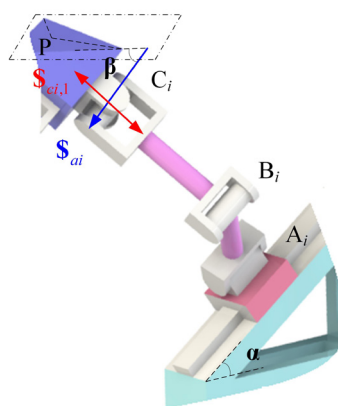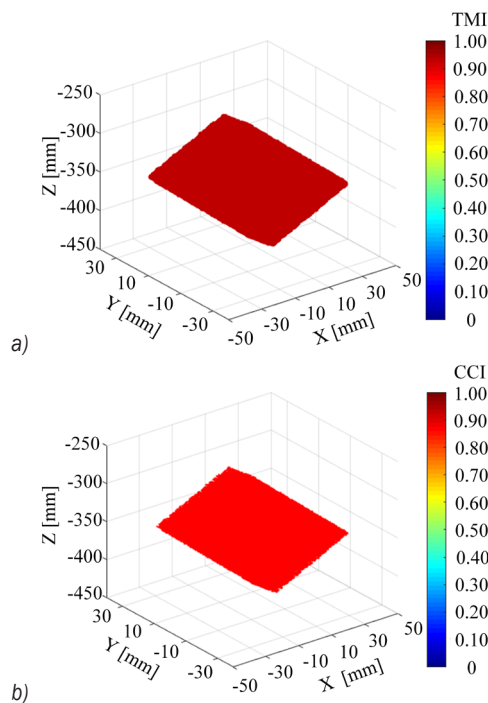
Fig. 9. a) Distribution of the TMI of 3-CRU PM when $\alpha = 25°$ and $\beta = 30°$, and b) distribution of the CCI of 3-CRU PM when $\alpha = 25°$ and $\beta = 30°$

When $\alpha=25°$ and $\beta=30°$, the distributions of TMI and CCI in the chosen spatial workspace can be obtained, as shown in Fig. 9. The workspace of 3-CRU PM is a regular hexahedron. The TMI and CCI of 3-CRU PM remain constant with values of 0.93 and 0.86, respectively. TMI is close to the maximum, which means that the TWSs exerted on the moving platform are almost same as that in the joint space when $\alpha=25°$. However, although CCI is slightly smaller than TMI, the distortion of CWSs exerted on the platform does not change that much. Angles α and β have influence on the force transmission manipulability and force constraint consistency of 3-CRU PM. Fig. 10 illustrates the relationship among TMI, CCI, α and β.

a)

b)

c)
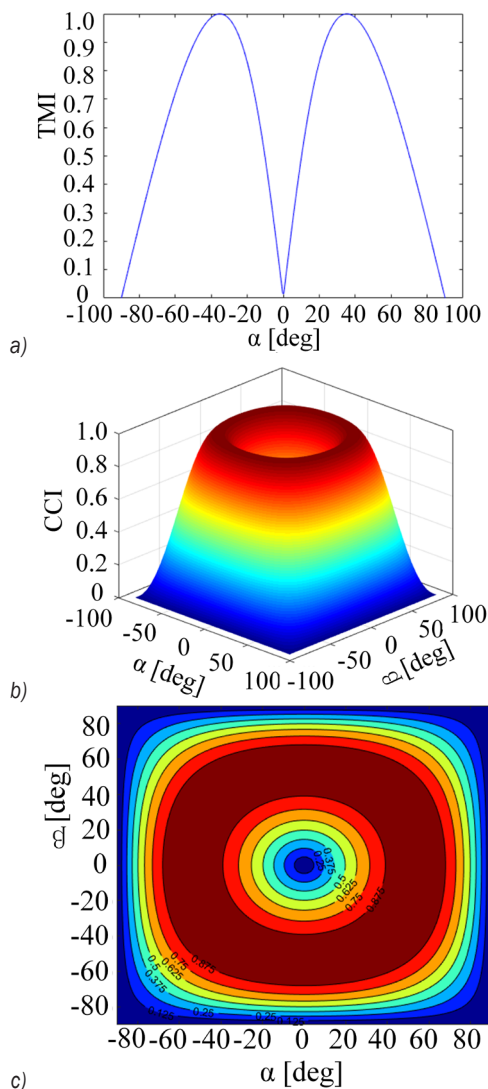
Fig. 10. *a) Relationship between TMI and α,
b) relationship between CCI and α as well as β,
c) contour of the relationship between CCI and α as well as β*

In Fig. 10a, TMI has a rapid increase with α when $\alpha \in [0°, 35.26°]$. When $\alpha=35.26°$, the index reaches the maximum and the TWSs exerted on the moving platform have no distortion, which means that the manipulability of transmission force is excellent. From Figs. 10b and c, it can be determined that the curved surface is on $\alpha=0°$ and $\beta=0°$ symmetry. When $\alpha \in [39.00°, 68.00°]$ and $\beta \in [39.00°, 68.00°]$, CCI is more than 0.88. That is to say, the CWSs exerted on the moving platform have less distortion. It should be noted that TMI and CCI equal to 1 and reach the maximum at the same time when $\alpha=35.26°$ and $\beta=45°$, which means that the transmission force vector and constraint force couple both have no "elastic" variation. The manipulability of transmission force and the consistency of constraint force are excellent and do not vary with the pose. The structural configuration of the PM corresponding to this case is presented in Fig. 11.
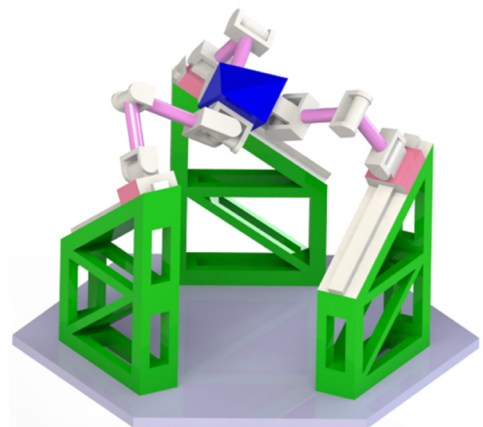
Fig. 11. *Structural configuration of the 3-CRU PM when TMI=1 and CCI=1*

4 MERITS OF TMI AND CCI

In summary, as compared with some other evaluation indices based on Jacobian matrix, the proposed indices TMI and CCI have the following merits:

TMI and CCI are dimensionless and frame-independent, so that the biased measure for the same PM caused by the selection of different reference coordinate frames can be avoided.

TMI and CCI range from 0 to 1, which results in intuitive measurement and comparison without interference from other factors of the PM (i.e., different rod lengths).

The proposed index CCI evaluates the quality of constraint force of lower-mobility PMs. In most cases, researchers only consider the mobility

property of the lower-mobility PM. That is to say, as long as the movement in the direction of non-mobility is constrained, the quality of the constraint is often ignored. The proposed CCI could evaluate the consistency of constraint force to resist deformation, achieving a more comprehensive evaluation of lower-mobility PMs.

5 CONCLUSIONS

Two new indices, TMI and CCI, are proposed to evaluate the manipulability to transmit force and the consistency to resist deformations, with the corresponding formulas being derived respectively under the conditions that the transmission matrix and constraint matrix are composed of linear force vectors, force couples, or both. These two indices stand out with the merits of unit homogeneity, frame independence and measurement facility without interference. Then, TMI and CCI are applied to 4-URU PM with mixed-motion PM, 2-UPR+SPR PM with parasitic motion and pure translational 3-CRU PM. The manipulability of transmission force and the consistency of constraint force of these PMs are evaluated. Moreover, the structural configuration of the 3-CRU PM whose TMI and CCI remain maximal is constructed for the first time, which means that the TWS and CWS exerted on the moving platform both have no distortion and achieve best manipulability and consistency in the whole workspace.

6 ACKNOWLEDGEMENTS

7 REFERENCES

[1] Merlet, J. (2006). *Parallel robots (Solid Mechanics and Its Applications, Vol. 2)*. Springer-Verlag, Dordrecht.

[2] Mei, J., Zang, J., Ding, Y., Xie, S., Zhang, X. (2017). Rapid and automatic zero-offset calibration of a 2-DOF parallel robot based on a new measuring mechanism. *Strojniški vestnik - Journal of Mechanical Engineering*, vol. 63, no. 12, p. 715-724, **DOI:10.5545/sv-jme.2017.4529**.

[3] Cheng, G., Gu, W., Yu, J., Tang, P. (2011). Overall structure calibration of 3-UCR parallel manipulator based on quaternion method. *Strojniški vestnik - Journal of Mechanical Engineering*, vol. 57, no. 10, p. 719-729, **DOI:10.5545/sv-jme.2010.167**.

[4] Cheng, G., Xu, P., Yang, D., Li, H., Liu, H. (2013). Analyzing kinematics of a novel 3CPS parallel manipulator based on Rodrigues parameters. *Strojniški vestnik - Journal of Mechanical Engineering*, vol. 59, no. 5, p. 291-300, **DOI:10.5545/sv-jme.2012.727**.

[5] Denavit, J., Hartenberg, R., Razi, R., Uicker, J. (1965). Velocity, acceleration, and static-force analyses of spatial linkages. *Journal of Applied Mechanics-Transactions of the ASME*, vol. 32, no. 4, p. 903-910, **DOI:10.1115/1.3627334**.

[6] Yoshikawa, T. (1985). Manipulability of robotic mechanisms. *The International Journal of Robotics Research*, vol. 4, no. 2, p. 3-9, **DOI:10.1177/027836498500400201**.

[7] Gosselin, C., Angeles, J. (1991). A global performance index for the kinematic optimization of robotic manipulators. *Journal of Mechanical Design*, vol. 113, no. 3, p. 220-226, **DOI:10.1115/1.2912772**.

[8] Merlet, J. (2006). Jacobian, manipulability, condition number and accuracy of parallel robots. *Journal of Mechanical Design*, vol. 128, no. 1, p. 199-206, **DOI:10.1115/1.2121740**.

[9] Wang, J., Liu, X., Wu, C. (2009). Optimal design of a new spatial 3-DOF parallel robot with respect to a frame-free index. *Science in China Series E Technological Sciences*, vol. 52, p. 986-999, **DOI:10.1007/s11431-008-0305-4**.

[10] Alt, H. (1932). Der ubertragungswinkel und seine bedeutung fur das konstruieren periodischer getriebe. *Werkstatttechnik*, vol. 26, p. 61-64.

[11] Sutherland, G., Roth, B. (1973). A transmission index for spatial mechanisms. *Journal of engineering for industry-Transactions of the ASME*, vol. 95, no. 2, p. 589-597, **DOI:10.1115/1.3438195**.

[12] Tsai, M., Lee, H. (1994). Generalized evaluation for the transmission performance of mechanisms. *Mechanism and Machine Theory*, vol. 29, no. 4, p. 607-618, **DOI:10.1016/0094-114X(94)90098-1**.

[13] Wang, J., Wu, C., Liu, X. (2010). Performance evaluation of parallel manipulators: motion/force transmissibility and its index. *Mechanism and Machine Theory*, vol. 45, no. 10, p. 1462-1476, **DOI:10.1016/j.mechmachtheory.2010.05.001**.

[14] Liu, H., Huang, T., Kecskeméthy A, Chetwynd, D., Li, Q. (2017). Force/Motion transmissibility analyses of redundantly actuated and overconstrained parallel manipulators. *Mechanism and Machine Theory*, vol. 109, p. 126-138, **DOI:10.1016/j.mechmachtheory.2016.11.011**.

[15] Meng, Q., Xie, F., Liu, X., Takeda, Y. (2020). Screw theory-based motion/force transmissibility analysis of high-speed parallel robots with articulated platforms. *Journal of Mechanisms and Robotics-Transactions of the ASME*, vol. 12, no. 4, p. 041011, **DOI:10.1115/1.4046031**.

[16] Brinker, J., Corves, B., Takeda, Y. (2018). On the motion/force transmissibility and constrainability of Delta parallel robots. *Computational Kinematics. Mechanisms and Machine Science*, p. 340-348, **DOI:10.1007/978-3-319-60867-9_39**.

[17] Wang, C., Zhao, T., Li, E., Zhao, Y., Bian, H. Zhu, B. (2021). A novel index to evaluate the mapping of parallel mechanisms from internal to external wrenches. *Mechanism and Machine Theory*, vol. 155, art. ID 104058, **DOI:10.1016/j.mechmachtheory.2020.104058**.

[18] Wang, X., Guo, W., Han, Y. (2020). A new index of static actuation force sensitivity of mechanisms based on unified forward Jacobian matrix. *Journal of Mechanisms and*

Robotics-Transactions of the ASME, vol. 12, no. 6, p. 1-30, **DOI:10.1115/1.4046976**.

[19] Utenov, M., Sobh, T., Baigunchekov, Z., Zhilkibayeva, S., Patel, S. (2018). Analytical method for determination of internal forces of mechanisms and manipulators. *Robotics*, vol. 7, no. 3, art. ID 53, **DOI:10.3390/robotics7030053**.

[20] Liang, X., Takeda, Y. (2019). Transmission index of a class of parallel manipulators with 3-RS(SR) primary structures based on pressure angle and equivalent mechanism with 2-SS chains replacing RS chain. *Mechanism and Machine Theory*, vol. 139, p. 359-378, **DOI:10.1016/j.mechmachtheory.2019.04.018**.

[21] Angeles, J. (2006). *Fundamentals of Robotic Mechanical Systems: Theory, Methods, and Algorithms*. Springer Verlag, Berlin.

[22] Angeles, J., López-Cajún, C.S. (1992). Kinematic isotropy and the conditioning index of serial robotic manipulators. *International Journal of Robotics Research*, vol. 11, no. 6, p. 560-571, **DOI:10.1177/027836499201100605**.

[23] Chablat, D., Angeles, J. (2007). On the kinetostatic optimization of revolute-coupled planar manipulators. *Mechanism and Machine Theory*, vol. 37, no. 4, p. 351-374, **DOI:10.1016/S0094-114X(01)00081-7**.

[24] Liu, Y., Xu, Y., Lyu, Y., Song, W. (2019). Kinematic performance analysis and scale optimization of a fully symmetric 4-URU parallel mechanism. *Journal of Mechanical Transmission*, vol. 29, no. 4, p. 35-40.

[25] Huang, Z., Zhao, Y., Zhao, T. (2014). *Advanced Spatial Mechanism* (2nd ed). High Education Press, Beijing. (in Chinese)

[26] Neumann, K. (2008). Adaptive in-jig high load Exechon machining & assembly technology. *Aerospace Manufacturing and Automated Fastening Conference & Exhibition*, p.08AMT-0044.

[27] Tang, T., Zhao, Y., Zhang, J., Jin, Yan. (2015). Conceptual design and workspace analysis of an Exechon-inspired parallel kinematic machine. Ding, X., Kong, X., Dai, J. (eds.), *Advances in Reconfigurable Mechanisms and Robots II*. Springer, Berlin, p. 445-453, **DOI:10.1007/978-3-319-23327-7_39**.

[28] Zhao, Y., Cao, Y., Kong, X., Zhao, T. (2018). Type synthesis of parallel mechanisms with a constant Jacobian matrix. *Journal of Mechanisms and Robotics-Transactions of the ASME*, vol. 12, no. 6, art. ID 061011, **DOI:10.1115/1.4040962**.